A POD-based analysis of turbulence in the reduced nonlinear dynamics system

2016 J. Phys.: Conf. Ser. 708 012002

(http://iopscience.iop.org/1742-6596/708/1/012002)

Journal of Physics: Conference Series **708** (2016) 012002 doi:10.1088/1742-6596/708/1/012002

A POD-based analysis of turbulence in the reduced nonlinear dynamics system

M-A Nikolaidis[1], B F Farrell[2], P J Ioannou[1], D F Gayme[3], A Lozano-Durán[4], J Jiménez[4]

[1]University of Athens, Department of Physics, Panepistimiopolis, Zografos, 15784 Athens, Greece
[2]Department of Earth and Planetary Sciences, Harvard University, Cambridge, MA 02138, USA
[3]Department of Mechanical Engineering, Johns Hopkins University, Baltimore, MD 21218, USA
[4]School of Aeronautics, Universidad Politécnica de Madrid, 28040 Madrid, Spain

E-mail: pjioannou@phys.uoa.gr

Abstract. The structure of turbulence in a reduced model of turbulence (RNL) is analyzed by means of a Proper Orthogonal Decomposition (POD modes). POD analysis was carried out on two different components of the flow, the roll/streak and the perturbation structure. The POD structure in both RNL and direct numerical simulations (DNS) is similar and this correspondence suggests that the dynamics retained in RNL are the essential dynamical ingredients underlying the self-sustaining mechanism of the turbulent state.

1. Introduction

Proper Orthogonal Decomposition (POD) provides an orthogonal basis for the spatial structure, each component of which is ordered according to its contribution to the variance of the flow. This basis is optimally efficient for representing the variance in turbulent flows and allows a systematic reduction in complexity of the representation of the flow. The POD analysis can be performed separately on components of the flow in homogeneous directions including the streamwise-mean component of the flow (with streamwise wavenumber $k_x = 0$) and the streamwise-varying components of the flow with $k_x \neq 0$ [1–4]. In this work we exploit this freedom to efficiently identify the structures that dominate the spatio-temporal variability of the streamwise-mean flow as well as the structures that dominate the streamwise-varying $k_x \neq 0$ components. POD modes obtained from DNS are compared with those obtained from a closely related reduced nonlinear (RNL) model [5]. The purpose of this comparison is in part to elucidate the similarities and differences of the DNS with the RNL. The dynamics of RNL model turbulence involve interaction of the streamwise mean flow with few, even as few as one, streamwise flow harmonic. Despite this simplification, salient aspects of the turbulent dynamics are captured [6–8]. Given the similarity between the structures that dominate the variance in DNS and RNL turbulence, it is argued that RNL and DNS turbulence are sustained by a dynamically similar mechanism. RNL turbulence self-sustains through interaction between the time-dependent $k_x = 0$ roll/streak structure with the streamwise varying flow components through a parametric time-dependent instability mechanism. It is argued that the same type of dynamics are responsible for sustaining DNS turbulence.

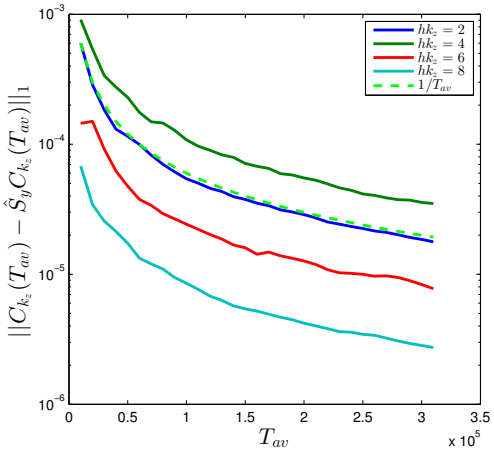

Figure 1. The 1-norm of the difference $C_{k_z} - \hat{S}_y C_{k_z}$ between the covariance matrix C_{k_z} (6), and the covariance of the reflected flow about the $x-z$ plane (B.5), at the center of the flow ($y = 1$) as a function of the averaging time, T_{av}, for $hk_z = 2, 4, 6, 8$ (top to bottom). This plot verifies that reflection symmetry about the centerline is a statistical symmetry of the flow and that this symmetry is approached at the rate $1/T_{av}$ consistent with the law of large numbers for quadratic statistics. Time is non-dimensionalized by h/U.

2. Procedure for obtaining the POD modes of the turbulent flow

Second-order statistics of flow structure can be obtained from the two-point same-time spatial covariance of the flow-field variables. Adopting the notation $\langle \cdot \rangle$ for the time average and $(\cdot)^T$ for transposition we form the covariance of the $k_x = 0$ components of the velocity,

$$C = \langle \mathcal{U}\mathcal{U}^T \rangle \ , \tag{1}$$

in which

$$\mathcal{U} = [U_s, V_s, W_s]^T \ , \tag{2}$$

is the column vector constructed of the deviations $(U_s(y,z,t), V_s(y,z,t), W_s(y,z,t))$ of the three components of the $k_x = 0$ Fourier mode of the streamwise (x), cross-stream (y) and spanwise (z) velocities $(U(y,z,t), V(y,z,t), W(y,z,t))$ from their spanwise averages, $([U](y,t), [V](y,t), [W](y,t))$.

In addition we form the covariance of the $k_x \neq 0$ components of the flow field,

$$c = \langle \mathcal{U}'\mathcal{U}'^{\mathcal{T}} \rangle , \tag{3}$$

with

$$\mathcal{U}' = [u, v, w]^T, \tag{4}$$

the column of the three components of the $k_x \neq 0$ Fourier component of the flow velocity expanded at all points of the domain.

The POD basis is obtained by eigenanalysis of the two-point covariances, C and c, of velocity components. The resulting orthogonal set of eigenvectors is then ordered descending in the magnitude of their eigenvalue to form the POD basis. The eigenvalue of each POD reveals its time-averaged contribution to the energy of the flow.

We have chosen for the study a plane Poiseuille flow in a doubly periodic channel in the streamwise, x, and spanwise, z, direction of size $L_x/h = 4\pi$, $L_z/h = \pi$, where h is the channel's half-width in the wall-normal direction, y, in which $\mathrm{Re}_\tau = 100$ is retained in both the DNS and

its reduced nonlinear model simulations (cf. Table 1). In order to obtain a converged POD basis a very long time series of a turbulent flow field is required. This convergence is facilitated by taking into account the statistical symmetries of the flow: homogeneity in the x and z direction, mirror symmetry in y about the $x-z$ plane at the center of the channel, and mirror symmetry in z about the $y-x$ plane at the center of the spanwise direction. The statistics of the turbulent flow have been verified to asymptote to the above statistical symmetries as the averaging time increases; convergence to the statistical symmetry is demonstrated for the case of the y mirror-symmetry in Fig. 1. These statistical symmetries are not necessary consequences of the translation and mirror symmetry of the NS equations in the periodic channel; the solutions may undergo symmetry breaking and be inhomogeneous either in x or z or mirror asymmetric. An example of symmetry breaking of the statistical homogeneity in the meridional direction is apparent in the nearly time invariant zonal flows that are maintained in the turbulent atmosphere of Jupiter. This symmetry breaking in the pipe flow would amount to a turbulent state with temporally constant and spatially fixed streak structures that are aligned parallel to the streamwise axis (cf. Ref. [9]).

Statistical homogeneity in z implies that the eigenvectors of C are single harmonics of the form:

$$\Phi_{k_z} = \begin{pmatrix} A_{k_z}(y) \\ B_{k_z}(y) \\ \Gamma_{k_z}(y) \end{pmatrix} e^{ik_z z} \ , \tag{5}$$

where $A_{k_z}(y)$, $B_{k_z}(y)$ and $\Gamma_{k_z}(y)$ are N_y dimensional column vectors, with N_y, the number of discretization points in y [2]. At each time instant the $3N_y$ column vector of a $k_z \neq 0$ Fourier component, $\mathcal{U}_{k_z}(t)$, of the instantaneous flow field $\mathcal{U}$ is obtained and used to form N_{k_z} average covariances:

$$C_{k_z} = \left\langle \mathcal{U}_{k_z}(t)\mathcal{U}^{\dagger}_{k_z}(t) \right\rangle \ , \tag{6}$$

where N_{k_z} is the number of $k_z \neq 0$ Fourier components retained in the simulation and $\dagger$ is the Hermitian transpose. Eigenanalysis of these covariances determines $3N_y \times N_{k_z}$ eigenvectors and the POD orthogonal basis of the $k_x = 0$ flow field is this basis ordered decreasing in eigenvalue.

The POD modes for the $k_x \neq 0$ component of the flow are obtained similarly. The eigenvectors of c are again single harmonics because of the statistical homogeneity in both x and z directions, of the form:

$$\phi_{k_x k_z} = \begin{pmatrix} \alpha_{k_x k_z}(y) \\ \beta_{k_x k_z}(y) \\ \gamma_{k_x k_z}(y) \end{pmatrix} e^{i(k_x x + k_z z)} \ , \tag{7}$$

where $\alpha_{k_x k_z}(y)$, $\beta_{k_x k_z}(y)$ and $\gamma_{k_x k_z}(y)$ are N_y dimensional column vectors. To obtain the POD basis we determine at each instant the $3N_y$ column vector corresponding to the $k_x \neq 0$, $k_z \neq 0$ Fourier component of $\mathcal{U}'_{k_x k_z}(t)$, of the instantaneous flow field $\mathcal{U}'$ and then form $N_{k_x} \times N_{k_z}$ average covariances:

$$c_{k_x k_z} = \left\langle \mathcal{U}'_{k_x k_z}(t)\mathcal{U}'^{\dagger}_{k_x k_z}(t) \right\rangle \ , \tag{8}$$

where N_{k_x} is the number of the $k_x \neq 0$ Fourier components retained in the simulation. Eigenanalysis of these covariances determines $3N_y \times N_{k_x} \times N_{k_z}$ eigenvectors and the POD orthogonal basis of the $k_x \neq 0$ flow field is this basis ordered decreasing in eigenvalue. A simpler calculation was carried out in this study, restricting the $k_x \neq 0$ components' POD analysis to a single plane, $y_n = 0.2066$. Note that because the physical flow field is real the Fourier components satisfy $\mathcal{U}_{-k_z} = \mathcal{U}^*_{k_z}$ where $*$ denotes the complex conjugate. Consequently $C_{k_z} = C^*_{-k_z}$ and covariances C_{k_z} and $C^*_{-k_z}$ have the same eigenvalues, as the covariances are positive definite Hermitian matrices with real eigenvalues. Their corresponding eigenfunctions

Table 1. Simulation parameters. $[L_x, L_z]/h$ is the domain size in the streamwise, spanwise direction. N_x, N_z are the number of Fourier components after dealiasing and N_y is the number of Chebyshev components. Re_τ is the Reynolds number of the simulation based on the friction velocity.

Abbreviation	$[L_x, L_z]/h$	$N_x \times N_z \times N_y$	Re_τ	Re
NS100	$[4\pi\ ,\ \pi]$	$128 \times 63 \times 97$	100.59	1650
RNL100	$[4\pi\ ,\ \pi]$	$3 \times 63 \times 97$	100.98	1950

are conjugate. This implies that the eigenvalues of the POD modes come in pairs corresponding to the $\sin(k_z z)$ and $\cos(k_z z)$ POD structure. When presenting the POD modes for each k_z only one of this pair will be shown. Similarly for the POD modes of the $k_x \neq 0$ flow field: there is a four-fold degeneracy corresponding to the common eigenvalues of $c_{k_x k_z}$, $c_{-k_x k_z}$, $c_{k_x -k_z}$, $c_{-k_x -k_z}$ and the POD modes can be represented with (x, z) structure either in the checkerboard form $\sin(k_x x)\sin(k_z z)$, $\cos(k_x x)\sin(k_z z)$, $\sin(k_x x)\cos(k_z z)$,$\cos(k_x x)\cos(k_z z)$, or in the oblique wave form: $\sin(k_x x + k_z z)$, $\cos(k_x x + k_z z)$, $\sin(k_x x - k_z z)$,$\cos(k_x x - k_z z)$, which will be chosen in our figures.

The complete set of POD modes form a basis orthogonal in the energy norm that spans the three components of the flow field. Although the POD basis is optimally efficient for representing perturbation energy, this basis is not optimal for representing the dynamics of the flow and care must be exercised in relating them to the dynamics of the turbulent state (for a discussion of the relation of the POD basis to the dynamics refer to Ref. [10]; construction of a basis for optimal representation of flow dynamics refer to Ref. [11]). In addition to non-optimality of the POD basis for representing dynamics is the potential for Galerkin projection of the dynamics using this basis to produce dynamical interaction inconsistent with NS which leads inter alia to support of unphysical instabilities [4]. What the POD basis does is to provide important information about flow structure that can be used to reconsrtuct the velocity fields with significantly lower degrees of freedom and therefore constrain the dynamics.

3. DNS and its RNL approximation

In this section we briefly describe the construction of the reduced nonlinear model (RNL) of Navier-Stokes plane channel turbulence. The incompressible Navier-Stokes equations in a constant mass-flux channel flow, with laminar flow in the streamwise x direction, is decomposed into equations for the streamwise average flow, $\mathbf{U}$, and the perturbations, $\mathbf{u}'$, as follows:

$$\partial_t \mathbf{U} + \mathbf{U}\cdot\nabla\mathbf{U} - G(t)\hat{\mathbf{x}} + \nabla P - \nu\Delta\mathbf{U} = -\overline{\mathbf{u}'\cdot\nabla\mathbf{u}'}\ , \tag{9a}$$

$$\partial_t \mathbf{u}' + \mathbf{U}\cdot\nabla\mathbf{u}' + \mathbf{u}'\cdot\nabla\mathbf{U} + \nabla\mathbf{p}' - \nu\Delta\mathbf{u}' = -(\mathbf{u}'\cdot\nabla\mathbf{u}' - \overline{\mathbf{u}'\cdot\nabla\mathbf{u}'})\ . \tag{9b}$$

$$\nabla\cdot\mathbf{U} = 0\ ,\quad \nabla\cdot\mathbf{u}' = 0\ . \tag{9c}$$

The pressure gradient $G(t)$ that drives the flow maintains constant mass flux. Quantities with an overline $\overline{\mathbf{u}'\cdot\nabla\mathbf{u}'}$ imply averaging over x. Capital letters indicate streamwise averaged quantities. No-slip, impermeable boundaries are placed at $y = 0$ and $y = 2h$.

The corresponding RNL equations are obtained by suppressing nonlinear interactions among streamwise non-constant flow components in the perturbation equations resulting in the right

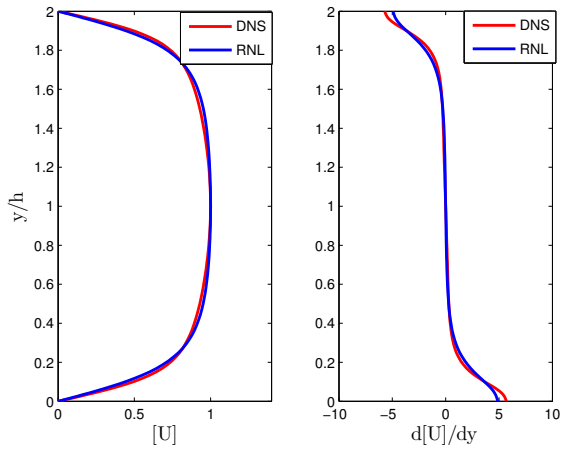

Figure 2. Left panel: The mean velocity profile of the DNS and RNL simulations. Right panel: The corresponding mean shear in the two simulations.

hand side of (9b) being set to 0. The RNL equations are:

$$\partial_t \mathbf{U} + \mathbf{U}\cdot\nabla\mathbf{U} - G(t)\hat{\mathbf{x}} + \nabla P - \nu\Delta\mathbf{U} = -\overline{\mathbf{u}'\cdot\nabla\mathbf{u}'}\ , \tag{10a}$$

$$\partial_t \mathbf{u}' + \mathbf{U}\cdot\nabla\mathbf{u}' + \mathbf{u}'\cdot\nabla\mathbf{U} + \nabla\mathbf{p}' - \nu\Delta\mathbf{u}' = 0\ . \tag{10b}$$

$$\nabla\cdot\mathbf{U} = 0\ , \quad \nabla\cdot\mathbf{u}' = 0\ . \tag{10c}$$

Under this restriction, the perturbation field interacts nonlinearly only with the mean, **U**, flow and not with itself. This quasi-linear restriction of the dynamics results in a turbulent state that is supported by a greatly restricted subset of streamwise Fourier components. The components that are retained by the dynamics identify the dynamically active components sustaining the turbulence. These components reveal the subset of streamwise harmonics that are are energetically active in the parametric instability that sustains the turbulent state [5–8].

Turbulence with realistic mean statistics is obtained with RNL dynamics even with the perturbation field further truncated to comprise a single wavenumber component. Simulations reported here retained only perturbations with streamwise wavelength $\lambda_x/h = 4\pi$, which correspond to the gravest streamwise mode in our computational channel of streamwise length $L_x/h = 4\pi$ and spanwise width $L_z/h = \pi$. These RNL simulations are compared with DNS simulations in this channel at $\mathrm{Re}_\tau = u_\tau h/\nu = 100$ with $u_\tau = \sqrt{\nu\,\mathrm{d}[U]/\mathrm{d}y|_\mathrm{w}}$ ($\mathrm{d}[U]/\mathrm{d}y|_\mathrm{w}$ is the shear at the wall) is the friction velocity. In order for the single component RNL simulation to obtain comparable Re_τ with DNS the pressure gradient is increased appropriately. If the perturbation field in the RNL were not constrained to a single streamwise component but were allowed to evolve until its natural support in streamwise wavenumbers had been obtained, it would have retained three streamwise components, with wavelengths $\lambda_x/h = 4\pi, 2\pi, 4\pi/3$, and would sustain turbulence with the Re_τ of the DNS without requiring adjustment of the pressure gradient. Numerical details can be found in Appendix A and a summary of the parameters of the simulations in Table 1. The time averaged streamwise mean flow $[U]$ and its associated shear in the DNS is shown in Fig. 2.

4. DNS and RNL POD modes

The POD basis for the $k_x = 0$ component of the flow in DNS and the RNL simulation will now be described. As explained earlier because of the statistical homogeneity of the flow in the z direction, these POD modes come in $\sin(k_z z)$ and $\cos(k_z z)$ pairs. The first 8 POD modes of the

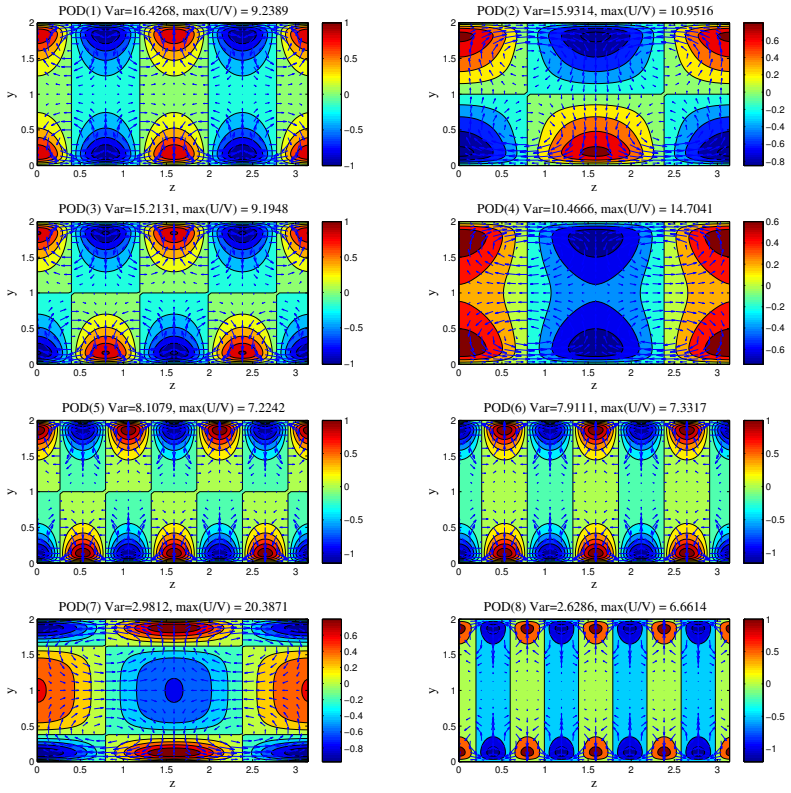

Figure 3. The first 8 POD modes of the turbulent channel flow. This basis has been obtained from data of a 270k advective (ht/U) time units simulation by exploiting the full symmetries of the flow as described in the text. There is a two-fold degeneracy such that each POD corresponds to two identical structures in y with $\sin(k_z z)$ and $\cos(k_z z)$ structure in z. The contours show levels of the streamwise U velocity and the arrows indicate the the vector velocity (V, W). These structures and this ordering was verified to be converged by doubling and quadrupling the averaging time.

DNS simulation are shown in Fig. 3 and the corresponding POD modes for the RNL simulation in Fig. 4. Shown are both the streak velocity and the corresponding (V, W) velocity field for each POD. Note that both the DNS and the RNL simulation produce rolls and streaks similarly collocated and with similar structure. The percentage variance explained by the first POD modes shown in Fig. 5 is similar in the DNS and RNL simulation.

Note that every POD component comes with its streamwise, wall-normal and spanwise velocity component. There is no a priori reason that these fields should be systematically correlated. However, a remarkable systematic correlation is seen between the wall-normal velocity V of the roll and the streak velocity: positive V is correlated with low speed streaks (defects in the streamwise flow) and vice versa. This correlation extends through to higher order POD modes. Each POD shows this remarkable correlation which indicates that the rolls and the streaks form a self-organized structure in which the lift-up mechanism is acting to maintain the streak. If instead the streaks were maintained directly by Reynolds stress forcing from the perturbation field no such systematic correlation between roll velocities and streak velocities would be expected. Analysis of the self-sustaining process (SSP) in RNL reveals that the streak is maintained by

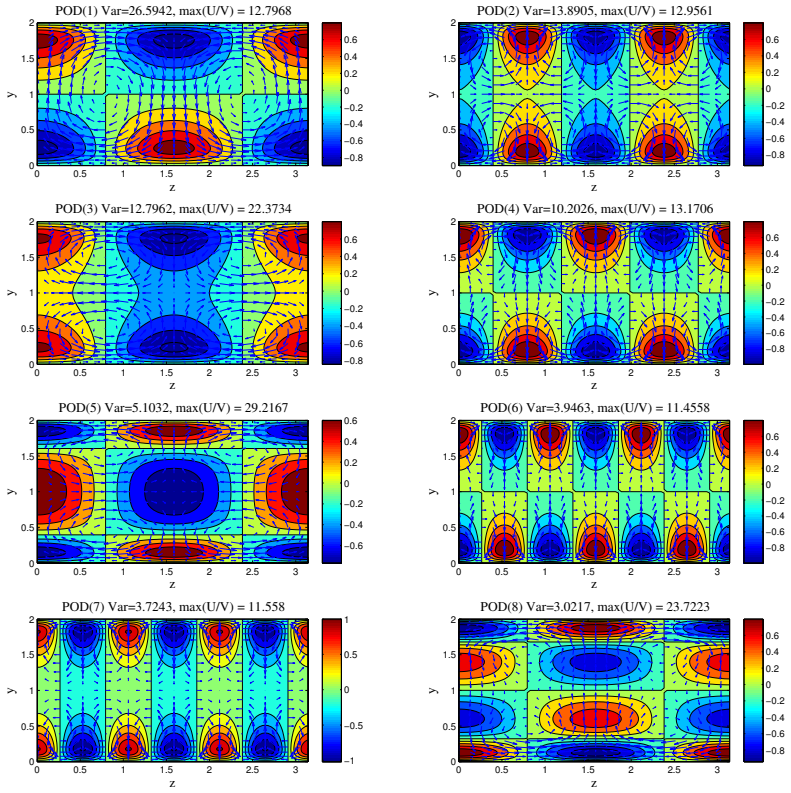

Figure 4. The first 8 POD modes of the turbulent channel flow under the corresponding RNL simulation as in Fig. 3.

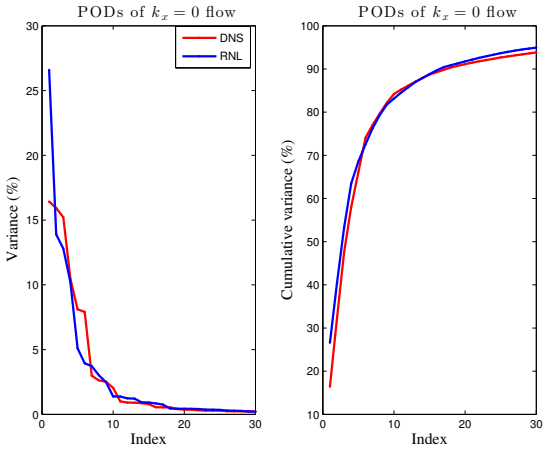

Figure 5. Left panel: Percentage energy (variance) of the $k_x = 0$ flow explained by each POD doublet in the DNS and RNL simulation. Right panel: The cumulative variance accounted for by the POD modes in the DNS and RNL simulation as a function of the number of POD modes included in the sum. The POD modes have been placed in descending order of the percentage variance that they account.

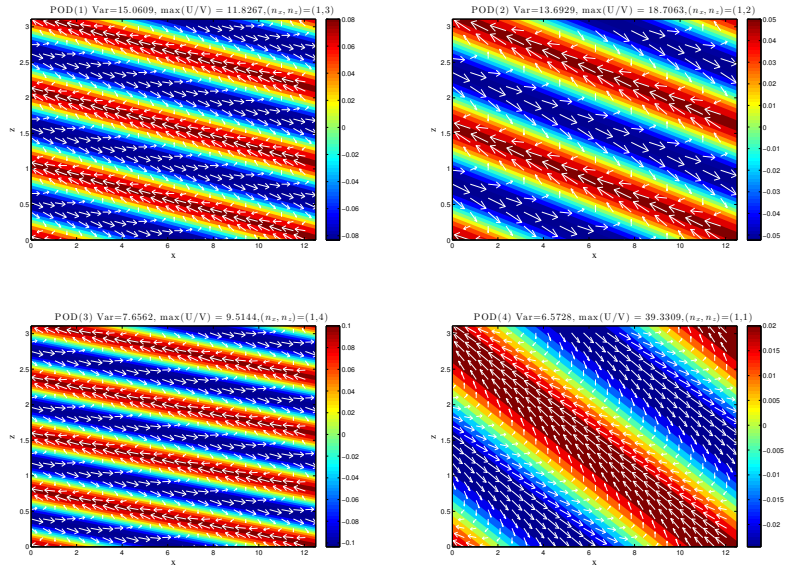

Figure 6. The first 4 POD modes of the DNS simulation at constant $y = 0.2066$. Contours are levels of the cross-flow velocity v' on the plane, while the arrows indicate the vector velocity (u', w') on the plane. Note that $u' > 0$ is associated with $v' < 0$ and vice versa an indication that the underlying dynamics are the lift-up mechanism as it operates in $k_x \neq 0$ perturbations.

the lift-up mechanism and that the eddies oppose the streak rather than maintain it. Note that the first 6 DNS POD modes of the roll/streak structure are reproduced in the RNL model, albeit with some reordering. The similarity of the RNL and DNS POD modes suggests that the same dynamics is operating and that the rolls and streaks self-organize so that the rolls form where the streaks are, in such a manner so as to reinforce the preexisting streak structure. This mechanism is evidently scale independent given that all the POD modes have this roll/streak velocity correlation. This scale independence suggests that the mechanism of maintaining the roll/streak structure is also scale independent.

The wall-normal V velocities of the roll component of the POD modes are about 1/10 of the streak velocity which, assuming an average non-dimensional mean flow shear of magnitude 2 (cf. Fig. 2) is consistent with the emergence of the streak through the lift-up mechanism over an average 5 time units. Note that in the RNL the streak/roll velocity ratio increases, which is to be expected because RNL turbulence is less disrupted due to having far fewer perturbation structures and streaks can reach larger amplitude.

We now consider the $k_x \neq 0$ POD modes of the flow. These assume the form of harmonics in x and z given the statistical homogeneity in x and z and there is fourfold degeneracy in the POD spectrum as each of the four combinations of waves $(\pm k_x, \pm k_z)$ accounts for the same amount of energy. These POD modes were calculated at $y = 0.2066$. A plane wave representative of the top 4 POD quartets for the DNS and the RNL are shown in Fig. 6 and Fig. 7 and the variance accounted by the POD modes is shown in Fig. 8. As the RNL simulation was restricted to a single mode, $hk_x = 0.5$, the RNL and DNS POD sets are not as similar as they would be if the full support of RNL turbulence had been retained. Nevertheless, the first 4 POD quartets of both the RNL and the DNS are $hk_x = 0.5$ structures. For the RNL we can see in Table 3 that

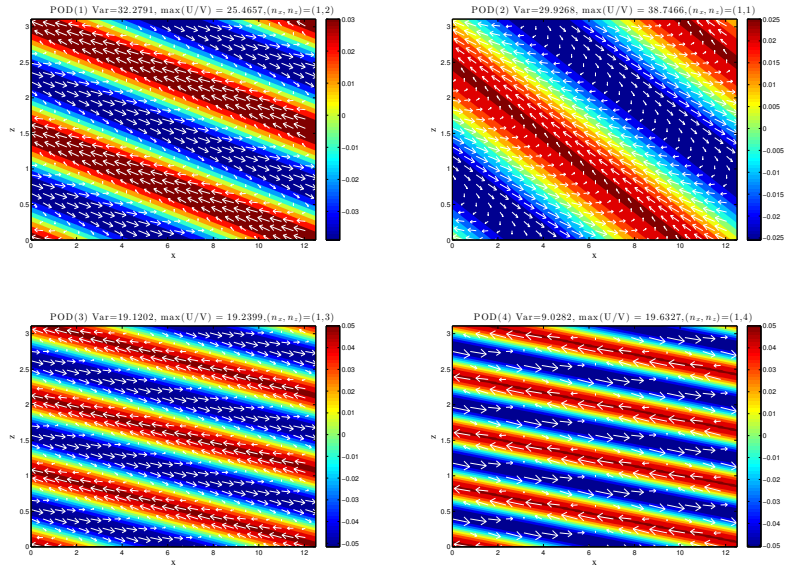

Figure 7. The first 4 plane POD modes of the RNL simulation as in Fig. 6.

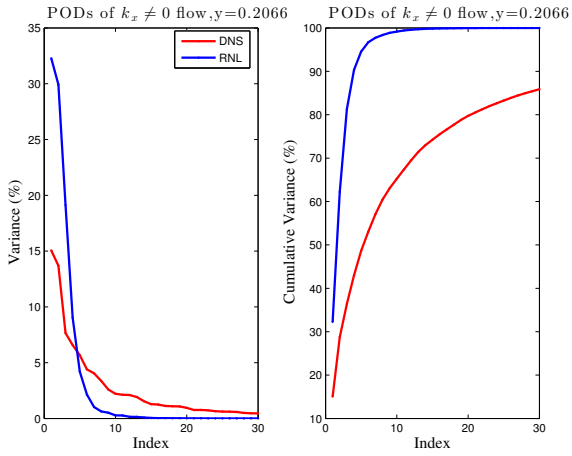

Figure 8. Left panel: Percentage energy (variance) of the $k_x \neq 0$ flow explained by each POD quartet in the DNS and RNL simulation. Right panel: The cumulative variance accounted for by the POD modes in the DNS and RNL simulation as a function of the number of POD modes included in the sum.

over 90% of the variance is explained by the first 4 modes, in fact the structure of the $hk_x = 0.5$ mode formed by using the first ten POD modes explains 99% of the variance. As expected, the DNS is more varied,with the $hk_x = 1$ mode making a comparable contribution (cf. Table 2).

As in the the case of the POD's at $k_x = 0$ the velocities u' and v' are correlated indicating that the lift-up mechanism is again at work, here however the lift-up mechanism is "supercharged" by the Orr-mechanism, which creates enhanced wall-normal velocity as the perturbations are sheared [12–15]. This supercharging mechanism associated with the eruptions in the flow does not operate at $k_x = 0$ and is distinct from the lift-up mechanism at $k_x = 0$. This distinction between the lift-up mechanisms operating at $k_x = 0$ and $k_x \neq 0$ is reflected in the ratio of the u'/v' of the POD modes being approximately double the U/V ratio in the $k_x = 0$ POD modes.

Table 2. POD modes of $y = 0.2066$ plane for DNS

Index	$(\pm)n_x$	$(\pm)n_z$	Variance(%)	Cumulative Variance(%)
1	1	3	15.06	15.06
2	1	2	13.69	28.75
3	1	4	7.66	36.41
4	1	1	6.57	42.98
5	2	3	5.67	48.65
6	2	2	4.40	53.05
7	2	4	4.04	57.09
8	1	5	3.37	60.46
9	3	3	2.60	63.06
10	2	1	2.21	65.27

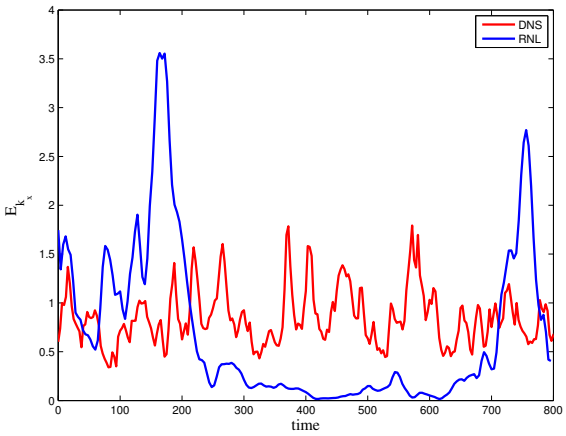

Figure 9. A segment of the energy time-series of $hk_x = 1$ on the plane $y = 0.2066$.

Also note that because the supercharge lift-up mechanism operating in the $k_x \neq 0$ perturbations scales inversely with the square of the total wavenumber of the perturbations the induced u' is larger for the lower wavenumber POD modes (cf. Refs. [12, 15]).

Due to the statistical homogeneity, the $k_x \neq 0$ POD modes of individual planes give information only about the relations between the velocity fields in the assumed single wave harmonic form. In order to obtain an understanding of the perturbation structure it is necessary to project the instantaneous flow on the POD basis. The time evolution of the perturbation energy at the $y = 0.2066$ plane for a segment of the DNS and RNL simulation is shown in Fig. 9. Figure 10 shows 2 instantaneous snapshots of the perturbation structure projected on the top 10 POD modes of the $hk_x = 0.5$ basis, at the start of an energy rising event in the DNS and RNL simulation. Regions of $u'v' < 0$ with alternating v' and u' signs are collocated with the most prominent streak defects which in both cases are negative. On this plane the interaction of the streak with the perturbations is connected with the product $w'\partial_z U_s$, generating perturbation velocity in the process. The perturbation structure consists of oblique waves at the wings of the spanwise shear of the streak.

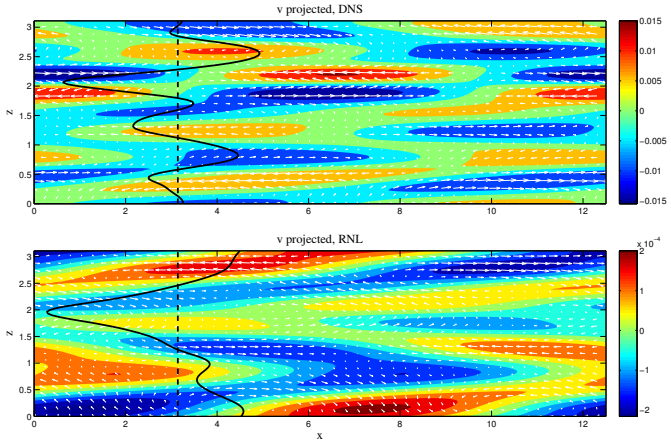

Figure 10. Instantaneous velocity fields of DNS and RNL projected on the first 10 POD quartets with $hk_x = 1$,showing the onset of an energy growth event. The contours show levels of the wall-normal velocity, the arrows the (u, w) vectors of the perturbation field on the plane $y = 0.2066$. The black dashed line at $x = \pi$ is the 0 of the streak, U_s, at this plane and the black solid line is 10 times the value of the streak velocity U_s. DNS is taken from time= 356 and RNL from time= 704. The corresponding perturbation energy is shown in Fig. 9.

Table 3. POD modes of $y = 0.2066$ plane for RNL

Index	$(\pm)\ n_x$	$(\pm)\ n_z$	Variance (%)	Cumulative Variance (%)
1	1	2	32.28	32.28
2	1	1	29.93	62.21
3	1	3	19.12	81.33
4	1	4	9.03	90.35
5	1	5	4.20	94.55
6	1	6	2.14	96.70
7	1	7	1.03	97.73
8	1	1	0.63	98.34
9	1	8	0.51	98.87
10	1	2	0.28	99.15

5. Further truncation of the RNL dynamics

The possibility of reducing the RNL dynamics support even further by using projection on the POD's will now be examined. Projection on a basis comprised of all three components (U_s, V, W) is constraining the dynamics in an undesirable way, since the streak $U_s \equiv U - [U]$ is the result of the (V, W) operating on the mean profile $[U]$ and the U_s itself. Therefore the streak dominated POD modes would not be able to correctly describe the roll dynamics since any roll is instantaneously associated with a much bigger streak [4]. For this reason we calculate the POD modes of only the streak portion of the flow and inquire whether we can obtain self-sustaining turbulence with a low order POD representation of the streak structure. It could be argued that a single pair of the POD basis cannot describe correctly the dynamics of the flow, since it would enforce symmetry between high and low speed streaks, and the mean flow would be consequently characterized by a nearly laminar unblunted profile.

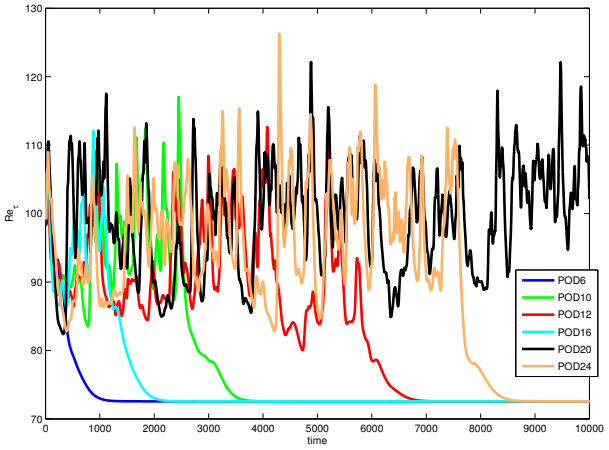

Figure 11. Friction Reynolds number Re_τ as a function of advective time for simulations truncating streak velocity U_s to 6, 10, 12, 16, 20 and 24 POD pairs.

Figure 11 shows the time series of Re_τ in simulations with a selection of POD pairs used for the truncation. The RNL system is otherwise unmodified in comparison to the one used for the calculation of the POD basis. When the lowest number of POD pairs is retained, the simulation laminarizes without exhibiting any dynamical behavior. An increase in the number of POD modes allows the system to retain its turbulent behavior. The lifetime of each simulation appears to be uncorrelated with the increase of the POD pair number. This suggests that the truncation likely does not cause relaminarization due to failure to represent the energy of the streak, which would be expected to produce laminarization far more quickly.

6. Discussion

Numerical data were obtained from a DNS of a turbulent channel and the corresponding RNL simulation. POD analysis was carried out on two different components of the flow, the roll/streak and the perturbation structure. Striking resemblance of the relations between the velocity fields was seen in the two simulations. This correspondence suggests a similar dynamics is at work in maintaining turbulence in these systems. Remarkably, the mechanism maintaining turbulence in the RNL system has been comprehensively characterized [5–8]. The close correspondence in structure and dynamics between RNL and NS dynamics invites the exploitation of the comprehensively characterized RNL turbulence to advance understanding of NS turbulence in channel flow. In particular, the lift-up mechanism operating at $k_x = 0$ and the associated "supercharge" mechanism operating at $k_x \neq 0$ have been clearly seen operating in both RNL and DNS including using the POD projections. As a further probe of the mechanism of RNL turbulence the POD modes were used to truncate the $k_x = 0$ velocity fields in a different RNL simulation, showing that the system sustains at a fairly low number of POD modes. This result provides an even more reduced turbulent dynamics in terms of the dimension of its support than the already highly reduced RNL turbulence which operates realistically supported by a single streamwise wavenumber.

The purpose of this comparison is in part to elucidate the similarities and differences of the DNS with the RNL. The dynamics of RNL model turbulence involve interaction of the streamwise mean flow with few, even as few as one, streamwise flow harmonic. Despite this simplification salient aspects of the turbulent dynamics are captured [5–8].

Acknowledgments
This work was funded in part by the Second Multiflow Program of the European Research Council. Brian Farrell was also supported by NSF AGS-1246929. We would like to thank Daniel Chung for his reviewing comments.

Appendix A.

The data were obtained from a DNS of (10) and from the RNL that is directly associated with the DNS. Both the DNS and its directly associated RNL are integrated with no-slip boundary conditions in the wall-normal direction and periodic boundary conditions in the streamwise and spanwise directions. The dynamics were expressed in the form of evolution equations for the wall-normal vorticity and the Laplacian of the wall-normal velocity, with spatial discretization and Fourier dealiasing in the two wall-parallel directions and Chebychev polynomials in the wall-normal direction [16]. Time stepping was implemented using the third-order semi-implicit Runge-Kutta method.

Appendix B. Calculating covariances for symmetrical states

Symmetries in reflections in y about the centerline $x-z$ plane at $y=1$ and reflections in z about the $y-x$ plane at $z=\pi/2$ add in the time series of the simulation 3 independent combinations of $A_{k_z}(y)$, $B_{k_z}(y)$ and $\Gamma_{k_z}(y)$:

$$\hat{S}_y\Phi_{k_z} = \begin{pmatrix} A_{k_z}(-y) \\ -B_{k_z}(-y) \\ \Gamma_{k_z}(-y) \end{pmatrix} e^{ik_z z} \ , \hat{S}_z\Phi_{k_z} = \begin{pmatrix} A^*_{k_z}(y) \\ B^*_{k_z}(y) \\ -\Gamma^*_{k_z}(y) \end{pmatrix} e^{ik_z z} \ ,$$

$$\hat{S}_z\hat{S}_y\Phi_{k_z} = \begin{pmatrix} A^*_{k_z}(-y) \\ -B^*_{k_z}(-y) \\ -\Gamma^*_{k_z}(-y) \end{pmatrix} e^{ik_z z} \ . \tag{B.1}$$

To recalculate the additional covariances for the above arrangements of the velocity fields we can use the following separation of the covariance

$$C_{k_z} = \begin{pmatrix} C^{uu}_{k_z} & C^{uv}_{k_z} & C^{uw}_{k_z} \\ C^{vu}_{k_z} & C^{vv}_{k_z} & C^{vw}_{k_z} \\ C^{wu}_{k_z} & C^{wv}_{k_z} & C^{ww}_{k_z} \end{pmatrix} \ , \tag{B.2}$$

with $C^{u_iu_j}_{k_z} = (C^{u_ju_i}_{k_z})^\dagger$. In the following the k_z subscript will be omitted and instead of u_iu_j the superscript ij will be used. So the covariance is written as:

$$C = \begin{pmatrix} C^{11} & C^{12} & C^{13} \\ C^{21} & C^{22} & C^{23} \\ C^{31} & C^{32} & C^{33} \end{pmatrix} \ . \tag{B.3}$$

Reflections of the velocities in z result in the conjugation of each individual covariance, and placement of a minus sign in the w components of the covariance, so that:

$$\hat{S}_z C = \begin{pmatrix} (C^{11})^* & (C^{12})^* & -(C^{13})^* \\ (C^{21})^* & (C^{22})^* & -(C^{23})^* \\ -(C^{31})^* & -(C^{32})^* & (C^{33})^* \end{pmatrix} \ . \tag{B.4}$$

Reflections in y require to reverse the order of the row and column indexes in each individual covariance and if this operation is noted as $\hat{S}_y C^{ij} = C_R^{ij}$ we have:

$$\hat{S}_y C = \begin{pmatrix} C_R^{11} & -C_R^{12} & C_R^{13} \\ -C_R^{21} & C_R^{22} & -C_R^{23} \\ C_R^{31} & -C_R^{32} & C_R^{33} \end{pmatrix} . \tag{B.5}$$

Finally combined z and y reflections are obtained by the successive action of the individual operators on the initial covariance, and thus:

$$\hat{S}_z \hat{S}_y C = \begin{pmatrix} (C_R^{11})^* & -(C_R^{12})^* & -(C_R^{13})^* \\ -(C_R^{21})^* & (C_R^{22})^* & (C_R^{23})^* \\ -(C_R^{31})^* & (C_R^{32})^* & (C_R^{33})^* \end{pmatrix} . \tag{B.6}$$

References

[1] Moin P and Moser R D 1989 Characteristic-eddy decomposition of turbulence in a channel *J. Fluid Mech.* **200** 471–509

[2] Berkooz G, Holmes P and Lumley J L 1993 The proper orthogonal decomposition in the analysis of turbulent flows *Ann. Rev. Fluid Mech.* **25** 539–575

[3] Sirovich L, Ball K S and Keefe L R 1990 Plane waves and structures in turbulent channel flow *Phys. Fluids A* **2** 2217–2226

[4] Moehlis J, Smith T R, Holmes P and Faisst H 2002 Models for turbulent plane Couette flow using the proper orthogonal decomposition *Phys. Fluids* **14** 2493–2507

[5] Farrell B F and Ioannou P J 2012 Dynamics of streamwise rolls and streaks in turbulent wall-bounded shear flow *J. Fluid Mech.* **708** 149–196

[6] Thomas V, Lieu B K, Jovanović M R, Farrell B F, Ioannou P J and Gayme D F 2014 Self-sustaining turbulence in a restricted nonlinear model of plane Couette flow *Phys. Fluids* **26** 105112

[7] Constantinou N C, Lozano-Durán A, Nikolaidis M A, Farrell B F, Ioannou P J and Jiménez J 2014 Turbulence in the highly restricted dynamics of a closure at second order: comparison with DNS *J. Phys. Conf. Ser.* **506** 012004

[8] Thomas V, Farrell B F, Ioannou P J and Gayme D F 2015 A minimal model of self-sustaining turbulence *Phys. Fluids* **27** 105104

[9] Avsarkisov V, Hoyas S, Oberlack M and Garcia-Galache J P 2014 Turbulent plane Couette flow at moderately high Reynolds number *J. Fluid Mech.* **751** R1

[10] Farrell B F and Ioannou P J 1993 Stochastic forcing of the linearized Navier–Stokes equations *Phys. Fluids A* **5** 2600–2609

[11] Farrell B F and Ioannou P J 2001 Accurate low-dimensional approximation of the linear dynamics of fluid flow *J. Atmos. Sci.* **58** 2771–2789

[12] Farrell B F and Ioannou P J 1993 Optimal excitation of three-dimensional perturbations in viscous constant shear flow *Phys. Fluids A* **5** 1390–1400

[13] Farrell B F and Ioannou P J 1993 Perturbation growth in shear flow exhibits universality *Phys. Fluids A* **5** 2298–2300

[14] Jiménez J, Del Álamo J and Flores O 2004 The large-scale dynamics of near-wall turbulence *J. Fluid Mech.* **505** 179–199

[15] Jiménez J 2013 How linear is wall-bounded turbulence? *Phys. Fluids* **25** 110814

[16] Kim J, Moin P and Moser R 1987 Turbulence statistics in fully developed channel flow at low Reynolds number *J. Fluid Mech.* **177** 133–166